Extending MGS-TES Temperature Retrievals in the Martian Atmosphere up to 90 km: Retrieval Approach and Results

A. G. Feofilov[1,2], A. A. Kutepov[1,2], L. Rezac[3], M. D. Smith[4]

[1]{The Catholic University of America, 620 Michigan Ave., Washington D.C. 20064, USA}

[2]{NASA Goddard Space Flight Center, Mailcode 674, Greenbelt, MD 20771, USA}

[3] {Hampton University, Hampton, VA, 23668, USA}

[4]{NASA Goddard Space Flight Center, Mailcode 693, Greenbelt, MD 20771, USA}

Correspondence to: A. G. Feofilov (artem-feofilov@cua-nasa-gsfc.info)

Abstract

This paper describes a methodology for performing a temperature retrieval in the Martian atmosphere in the 50–90 km altitude range using spectrally integrated 15 μm CO_2 limb emissions measured by the Thermal Emission Spectrometer (TES), the thermal infrared spectrometer on board the Mars Global Surveyor (MGS). We demonstrate that temperature retrievals from limb observations in the 75-90 km altitude range require accounting for the non-local thermodynamic equilibrium (non-LTE) populations of the $CO_2(v_2)$ vibrational levels. Using the methodology described in the paper, we have retrieved ~1200 individual temperature profiles from MGS TES limb observations in the altitude range between 60 and 90 km. Our dataset of retrieved temperature profiles is available for download in supplemental materials of this paper. The temperature retrieval uncertainties are mainly caused by radiance noise, and are estimated to be about 2 K at 60 km and below, 4 K at 70 km, 7 K at 80 km, 10 K at 85 km, and 20 K at 90 km. We compare the retrieved profiles to Mars Climate Database temperature profiles and find good qualitative agreement. Quantitatively, our retrieved profiles are in general warmer and demonstrate strong variability with the following values for bias and standard deviations (in brackets) compared to the Martian Year 24 dataset of the Mars Climate Database: 6 (±20) K at 60 km, 7.5 (±25) K at 65 km, 9 (±27) K at 70 km, 9.5 (±27) K at 75 km, 10 (±28) K at 80 km, 11 (±29) K at 85 km, and 11.5 (±31) K at 90 km. Possible reasons for the positive temperature bias are discussed.

Keywords: temperature retrievals, middle atmosphere of Mars, remote sensing.

1. Introduction

The TES instrument on the MGS orbiter mapped the atmosphere of Mars for more than three Martian years allowing an unprecedented survey of the present Martian climate. The TES observations have been used to retrieve temperature profiles (Conrath et al. 2000), aerosol optical depth and physical properties (e.g. Pearl et al. 2001; Smith et al. 2001; Smith 2004; Clancy et al. 2003; Wolff and Clancy 2003), and water vapor abundance (Smith 2002; 2004). Most of the previously reported temperature retrievals from TES cover the atmosphere up to the ~0.01 mbar level, which corresponds to ~60 km altitude. However, in the limb observation mode measurements were performed at higher altitudes, up to ~120 km altitude. The upper limit for the currently available TES retrievals was set in accordance with the signal-to-noise ratio of the observations used in the constrained linear inversion algorithm applied for temperature retrievals (Conrath et al., 2000). In this work we used a stable forward-fitting temperature retrieval algorithm and applied it to a spectrally integrated CO_2 15 µm radiance to extend the upper altitude of temperature retrievals to 90 km and to provide the community with high-altitude temperature data for Martian Years (MY) 24 and 25. Temperature soundings in the middle atmosphere of Mars are important since they can provide important insight into the dynamics of the region that is linked with convective instabilities and gravity wave propagation and dissipation (e.g. Heavens et al., 2010 and references therein) and can provide additional constraints on tidal and gravity wave drag needed for modeling work (e.g. Forget et al., 1999; Forbes and Miyahara, 2006; Hartogh et al., 2007).

The structure of this paper is as follows: Section 2 describes the TES instrument. In Section 3 we discuss the details of the observed CO_2 15 µm band radiance including the breakdown of local thermodynamic equilibrium (LTE) at high altitudes and the effects of the upper atmosphere of Mars on simulated limb radiances. In Section 3 we also introduce the selection procedure we use on the observations and we define the integrated radiance that will be used for the retrievals. Section 4 describes the non-LTE retrieval code ALI-ARMS (see the Appendix for abbreviations not explained in the text), the temperature retrieval algorithm, and the retrieval uncertainties. In Section 5 we present the retrieved temperature profiles and compare them to averaged temperature profiles from the Mars Climate Database dataset. A discussion of similarities and differences is also included into this section. Finally, we present our conclusions in Section 6.

2. TES instrument

MGS began mapping operations from Mars orbit on 1 March 1999 (MY 24, Ls = 104°) and provided nearly continuous monitoring of conditions in the Martian atmosphere for over three full Martian years. The MGS mission ended on 2 November 2006 when the contact with the spacecraft

was lost. The TES instrument (Christensen et al. 2001) systematically measured and monitored the Martian surface and atmosphere throughout all phases of the mission. The imminent failure of a neon bulb required for calibration of the spectrometer forced spectrometer observations to end on 31 August 2004 (MY 27; Ls=81°), although observations continued using the TES bolometers. The near-polar solar-locked mapping orbit allowed 12 orbits per day of data at roughly 2:00 AM and 2:00 PM local time. A majority of observations were taken in the nadir geometry, but limb observations of the Martian atmosphere were included roughly every 10 degrees of latitude throughout the orbit (both day and night) throughout the mission. Each 8.3 mrad detector field-of-view had a projected size of about 13 km at the limb, allowing vertical resolution of just over a scale height. In a limb-geometry sequence, the 3x2 array of TES detectors scanned the atmosphere in overlapping steps from below the surface to about 120 km tangent height above the surface providing vertical sampling of about 1 to 5 km (see for more details in (Christensen et al., 2001)). The total number of limb geometry spectra obtained during the mission is about 750,000. In this work we show that a limited number of limb geometry spectra taken during the first Martian year have signal to noise ratio (SNR) that allows an extension of temperature retrievals up to 90 km altitude. The selection criteria for these spectra are described in Section 3.2.

3. CO_2 15 μm radiance measured by MGS-TES

In the gas phase, carbon dioxide (CO_2) molecular vibrations involve combinations of symmetric stretch (v_1), covalent bond bending (v_2), and asymmetric stretch (v_3) modes. The diagram in Fig. 1 shows the ground state and various excited vibrational levels of the CO_2 molecule up to an energy of 7445 cm^{-1}. The levels are marked in accordance with the Herzberg notation $v_1 v_2^l v_3$ where v_1, v_2, and v_3 denote the number of the corresponding vibrational quanta and the l symbol refers to the orbital quantum number. The 15 μm radiance measured by the TES instrument and used for temperature retrievals in this study arises from the optical transitions from vibrationally excited states with $\Delta v_2 = 1$, where Δv_2 denotes the change in the v_2 vibrational quanta number.

3.1. LTE and non-LTE conditions in CO_2 vibrational levels in the Martian atmosphere

The interpretation of TES 15 µm limb radiance profiles requires information on the populations of the corresponding CO_2 vibrational levels at the altitudes of the limb observations. In the lower atmosphere the frequency of inelastic molecular collisions is sufficiently high that these collisions overwhelm other population/depopulation mechanisms of the molecular vibrational levels. This leads to a local thermodynamic equilibrium, and the populations follow the Boltzmann distribution governed by the local kinetic temperature T_{kin}. In the upper atmosphere of Mars, where the frequency of inelastic collisions is much lower than that at lower altitudes, other processes also influence the population of CO_2 vibrational levels. These include: a) the direct absorption of solar radiance by the CO_2 vibrational-rotational bands in the 2.0, 2.7, and 4.3 µm spectral regions; b) absorption of the 15 µm radiance coming from the warmer and denser lower atmosphere; c) vibrational-translational (V–T) energy exchanges by collisions with molecules and atoms of other atmospheric constituents; and d) collisional vibrational-vibrational (V–V) energy exchange with other molecules. As a result, LTE no longer applies in this altitude region and the populations must be found by solving the self-consistent system of kinetic and radiative transfer equations, which express the balance relations between various excitation/de-excitation processes described above. The most important rate coefficient that defines the population of $CO_2(v_2)$ vibrational levels in the upper atmosphere of Mars is $k_{VT}\{CO_2\text{-}O\}$, the quenching rate coefficient for V–T energy exchange process at CO_2–O collisions (Ch. 10.3 in (López-Puertas and Taylor, 2001)). Despite the efforts of several different research groups, there is still a discrepancy between the laboratory measurements of this rate coefficient that provide low values of about 1.3–$1.5 \times 10^{-12}\,\mathrm{cm^3\,s^{-1}}$ (Pollock et al., 1993; Khvorostovskaya et al., 2002; Castle et al., 2006) and atmospheric retrievals that require $k_{VT}\{CO_2\text{-}O\} = 6.0 \times 10^{-12}\,\mathrm{cm^3\,s^{-1}}$ for an adequate interpretation of 15 µm CO_2 radiance (Sharma and Wintersteiner, 1990; Ratkowski et al., 1994; Gusev et al., 2006). The discussion of this problem is beyond the scope of this work, but its effect is minimized in this work because the $CO_2(v_2)$ vibrational level populations are in LTE up to ~80–90 km, and we utilize a "buffer zone" (see the end of Sect. 3.1 and Sect. 4) in the 90–100 km altitude range that compensates for the uncertainties in the upper part of the atmosphere including uncertainty in the $k_{VT}\{CO_2\text{-}O\}$ rate coefficient. The value $k_{VT}\{CO_2\text{-}O\} = 6.0 \times 10^{-12}\,\mathrm{cm^3\,s^{-1}}$ was used in all calculations performed for this work.

In this retrieval we used the non-LTE model developed in our group (Gusev, 2003; Kutepov et al., 2006). This model includes five CO_2 isotopes, 60 vibrational levels, and 20,000 optical transitions

from the HITRAN 2004 database (Rothman et al. 2005). It can easily be extended to include more levels and more transitions; however, this was not needed for the purposes of our work (see the discussion of the levels needed to be included into the task in Ch. 10.3 of (López-Puertas and Taylor, 2001)). The calculations and retrievals were performed using the ALI-ARMS research non-LTE code (see Section 4 below).

The calculations show that the main contributors to 15 µm radiance are the fundamental and first hot 15 µm CO_2 bands and that the corresponding 01^10 and 02^20 vibrational levels are in LTE below ~85 km altitude. Even though the area of our primary interest (60–90 km) doesn't demonstrate strong non-LTE features, performing non-LTE calculations is still required to take into account the contributions of the upper layers in the limb observation geometry. This is demonstrated in Fig. 2, where a reference profile of CO_2 15 µm radiance is compared with the CO_2 radiance profiles calculated using different approaches. The reference profile of non-LTE 15 µm radiance was estimated for the tropical atmosphere (lat = 0°), L_s=180° model extracted from the Mars Climate Database (MCD). We used pressure/temperature, CO_2, and O VMR profiles covering the 0–200 km altitude range. In this and other exercises we used the recommended MY 24 dust and average solar flux scenario dataset available for download at http://johnson.lmd.jussieu.fr:8080/las/servlets/dataset. Here and below we will refer to this dataset as simply the "MCD"). To obtain this profile we first calculated the non-LTE populations of the CO_2 vibrational levels at all heights and then calculated the limb radiance for each spectral line in the 560–770 cm^{-1} spectral interval and at each tangent height. After that, the radiance was spectrally integrated and the resulting integrated 15 µm radiance formed the reference profile. To demonstrate the importance of the accurate calculation of $CO_2(v_2)$ populations in the upper atmosphere for the limb radiance simulations below, we simulated limb radiance using LTE populations of vibrational levels (curve with circles in Fig. 2). As one can see, this significantly overestimates the radiance. In the course of the retrieval this approach would lead to underestimating the temperature down to 50 km altitude. One of the ways of dealing with this problem is by cutting out the upper atmosphere in the calculations to avoid the unrealistic radiance coming from the upper layers. Figure 2 shows the results of LTE and non-LTE runs when the atmosphere was cut out just above 100 km. As one can see, in these cases the radiance is underestimated above ~80 km altitude, which would lead to overestimating temperatures in the retrieval. Moving the upper limit of the atmosphere in the calculations, one can compensate for the non-LTE correction. However, this will introduce an uncontrolled uncertainty since the upper limit will depend on the atmospheric profile and individual non-LTE calculations will be required to find the corresponding altitude. On the other hand, using the full non-LTE model in combination with averaged atmospheric profiles in the upper

atmosphere helps to eliminate this problem. In addition (see Section 4), in our temperature retrievals we used the 90–100 km altitude interval as a "buffer zone" to compensate for possible deviations of the upper atmosphere profiles from the real ones. Temperature retrievals in the buffer zone are not included to the output product and are presented in data files only for control purposes: the stronger the gradient in the buffer zone, the larger the discrepancy of the simulated and measured profiles above 100 km altitude due to the uncertainties in this area.

3.2. MGS-TES spectra selection and processing

In this work we used spectrally integrated 15 μm CO_2 band radiance in the retrievals to increase SNR and to extend the upper limit of the retrieved temperature profile. In a sense, using the integrated radiance converts the spectrometer to a broadband radiometer like, for example, the SABER instrument (Russell et al., 1999) that was successfully used for temperature retrievals in the Earth's atmosphere up to ~110 km altitude. Spectra selection for integration and processing was based on two criteria: a limb sequence should a) provide a sufficient number of measured points above 60 km altitude and b) SNR for the integrated signal should be greater than unity up to at least 85 km. The calculations performed in this work show that both during the day and night in the Martian atmosphere, the 15 μm CO_2 band radiance is confined within the 560–770 cm^{-1} spectral range and all spectral line intensities in the 510–560 cm^{-1} and 770–830 cm^{-1} spectral windows are less than 1% of the line intensities in the maximum of the 15 μm manifold. Correspondingly, we have selected the former interval as the "information content" window and the two latter as "noise and bias" windows. To remove biases we fit for a second order polynomial using the spectral points in the "noise and bias" windows, and then we subtract the corresponding values from the "information content" spectral intensities. Examples of the resulting spectra in the 61–89 km altitude interval are shown in Fig. 3a–f. As one can see, the suggested procedure efficiently removes any bias at all considered altitudes. The integrated values of the 15-μm radiance in the 560–770 cm^{-1} spectral range are shown in Fig. 3g. This panel also contains the NER value estimated from observed signal values in the "noise and bias" windows. As one can see in Fig. 3g, the NER becomes comparable to the integrated signal at ~86 km altitude. The number of limb sequences for which the NER allows retrievals up to 90 km altitude is small compared with the total number of limb measurements. There are two reasons for that. First, the altitude coverage of limb measurements differs and not all limb sequences provide valid data points up to 90 km altitude. Second, the increasing noise in TES observations as the mission went on limits the limb scans with "good SNR" up to 90 km to the first two Martian years of the mission. Selecting high SNR scans may introduce a positive bias to the average retrieved temperature profile as we will show below in Sect. 5.2. However, this does not produce any errors in individual temperature

profiles that we have used for analysis. Overall, we have identified 1410 limb sequences that satisfy the SNR and altitude coverage criteria (see Fig. 4). All of these observations were processed using the retrieval procedure described in the next section.

4. ALI-ARMS research code and retrieval algorithm

All of the calculations performed in this work were made using the ALI-ARMS computer code (see Kutepov et al., 1998; Gusev, 2003; Gusev and Kutepov, 2003; and references therein) that solves the multi-level problem using the Accelerated Lambda Iteration (ALI) technique developed for calculating non-LTE populations of atomic and ionic levels in stellar atmospheres (Rybicki and Hummer, 1991). The code iteratively solves a set of statistical equilibrium equations and the radiative transfer equations. The algorithm efficiency is ensured by the ALI technique, which avoids the expensive radiative transfer calculations for the photons trapped in the optically thick cores of spectral lines. The ALI-ARMS model was successfully applied by Kaufmann et al. (2002; 2003) and Gusev et al. (2006) to the non-LTE diagnostics of spectral observations of the Earth's limb from the CRISTA instrument (Offermann et al., 1999; Grossmann et al., 2002). Kutepov et al. (2006) used this model to validate temperature retrievals from the 15 µm CO_2 emissions measured by the SABER instrument onboard the terrestrial TIMED satellite. Feofilov et al. (2009) used this code for the H_2O non-LTE model validation and H_2O VMR retrievals from the 6.3 µm H_2O emissions measured by SABER.

The retrieval method implemented in the ALI-ARMS code is similar to the iterative onion-peel technique using the relaxation method described in Gordley and Russell (1981). The process starts with an initial guess of a temperature profile combined with a fixed atmospheric model (pressure, VMRs of CO_2 and atomic oxygen retrieved from the MCD). The non-LTE populations are calculated and used for monochromatic limb radiance calculations for each limb path that is integrated and convolved with the MGS-TES field of view. The resulting simulated radiance I is compared to the measured radiance at each tangent height, and the temperature profile is iterated using the following relaxation scheme: $\xi^{i+1} = \xi^i + (I_{meas} - I^i) / (\partial I / \partial \xi)$, where ξ^{i+1} and ξ^i are the temperature values at the $i+1$-th and i-th iterations, respectively, I_{meas} is the integrated limb radiance measured by TES (see Section 3.2 above), I^i is the simulated limb radiance at the i-th iteration, and $(\partial I / \partial \xi)$ is the numerically calculated derivative of the radiance produced by the forward model with respect to ξ. After all limb paths have converged, a new temperature profile is produced, the hydrostatic equilibrium equation is solved for, the new non-LTE populations of CO_2 molecular levels are calculated, and the radiance is simulated again. The iterations are repeated until the

differences between the simulated and measured radiances become equal to or smaller than the radiance noise in the observed integrated limb radiance.

Figure 5 shows a self-consistency check of the retrieval procedure performed for the model atmosphere described above. First, the non-LTE task was solved for the reference temperature profile $T_{ref}(z)$, and the limb radiance was calculated using the non-LTE populations of the CO_2 levels, observation geometry, and TES field of view. Second, the resulting radiance profile was used as the "measured" profile $I_{meas}(z)$. Two tests were then conducted. The initial guess temperature profile $T(z)$ was set equal to $T_{ref}(z) - 30$ K (case I) and $T_{ref}(z) + 30$ K (case II) in the 60 – 90 km altitude range. Below 50 km and above 100 km the original values of the $T_{ref}(z)$ profile were used. In the 50–60 km and 90–100 km altitude ranges the temperature profiles were smoothly sewn together. The retrieval procedure was run for both cases. Figure 5a shows that the retrieved temperature profile rapidly converges to the reference profile in the course of a few iterations and that the result only slightly depends on the initial profile. This dependence is due to field of view averaging effects. To minimize the temperature uncertainty caused by these effects the retrieval procedure should comply with the following requirements: a) the initial guess $T(z)$ profile should not be unrealistically high or low. We recommend starting the retrieval from the climatological mean $T(z)$. b) The iterations should be stopped as soon as the convergence criterion is reached. Further fitting of radiance may lead to the appearance of false structures in the retrieved temperature profiles (Houghton et al, 1984, p.148). Figure 5b demonstrates the differences between the simulated and reference radiances after each iteration. One can see that the converged radiance profile reproduces the reference profile well at all points in the 60 – 90 km altitude range. We also performed runs similar to those described above but with noise added to $I_{meas}(z)$ and for different seasons and geographic locations. Noise levels were estimated from real data. This study provided the following temperature retrieval uncertainties: 2 K at 60 km and below, 4 K at 70 km, 7 K at 80 km, and 10 K at 85 km altitude.

5. Temperature retrievals from TES measurements

5.1. Input data and retrieval procedure

All the retrievals performed in this study utilized the retrieval algorithm described in Section 4. For each of the 1410 integrated TES radiance profiles (see Section 3.2) the initial guess atmospheric profile was assembled from pressure/temperature profiles in 10–60 km altitude range retrieved by the TES team using nadir geometry observations (Conrath et al. 2000; Smith 2004), and from pressure/temperature, CO_2 and O VMRs taken from the MCD in the 60–200 km interval. For each integrated radiance profile the retrieval procedure was run for 20 retrieval iterations. The retrieval was performed over the 50–100 km range with the 90–100 km interval used as a "buffer zone" to

smooth out the effects of limb radiance discrepancies in the upper atmosphere (see Section 3.1). The 50–60 km interval was included in the retrieval to allow for temperature profile adjustment in this area due to changes in the upper part. For each of the 20 iterations the root mean square (r.m.s.) of the radiance deviation ($I_{meas} - I_{calc}$) was calculated in the 60–90 km altitude range. For the majority of the profiles the minimum r.m.s. radiance deviation was reached between the 7th and 10th iteration. If convergence was not reached or the deviation of radiances at any altitude of the retrieval interval range was greater than 10% then the profile was not included to the output data. Approximately 14% of the profiles did not pass this test. We present the remaining 1214 temperature profiles in this work.

5.2. Retrieved temperature profiles

The complete set of individual temperature profile retrievals is available for download as an archive at http://cua-nasa-gsfc.info/feofilov/TES_HighAlt.zip. For a description of the dataset see the file "readme.txt" inside the archive. In this work we present some examples of individual retrievals and compare the averaged profiles with those from the MCD (using the standard MY 24 dust and average flux scenario).

Three examples of individual temperature profiles retrieved from integrated TES radiance are shown in Fig. 6a–c. As expected, below ~55 km they match the initial temperature profile. Above 60 km, the retrieved temperature profiles differ from the model and, in general, individual temperature retrievals show much higher variability than the model profiles. This may be explained by gravity waves in the Martian atmosphere, which are not reproduced in the model. Lack of temperature measurements in the Martian atmosphere for the period considered in the study prevents a profile-by-profile comparison with other instruments. Instead, we compare the zonally and seasonally (with a 30° step over L_s) averaged temperature profiles from TES retrievals with corresponding profiles from the MCD. We present 12 averaged temperature profiles in Figure 7. The profiles are marked in the figure caption with L_s counted from the year the mission has started (MY 24) so that L_s=390° corresponds to MY 25, L_s=30°. Each of the rows of panels in Fig. 7 contains three temperature distributions: high latitudes in the Southern Hemisphere, equatorial or mid-latitude, and high latitudes in Northern Hemisphere. Each displayed profile represents an average over ~10–15 individual retrieved profiles. As one can see, there is qualitative agreement between the retrieved temperature profiles and the MCD. However, absolute values differ and in some cases the difference may exceed 30 K. In general, our TES retrievals are warmer in the 60–90 km altitude range than the MCD temperature profiles. An analysis of our entire retrieval set in comparison to the MCD profiles gives the following values for bias and standard deviations (in brackets): 6 (±20) K at 60 km, 7.5 (±25) K at 65 km, 9 (±27) K at 70 km, 9.5 (±27) K at 75 km,

10 (±28) K at 80 km, 11 (±29) K at 85 km, and 11.5 (±31) K at 90 km. The temperature variability responsible for the standard deviations is expected since our TES retrievals represent individual profiles. The increase of standard deviation with altitude can be explained by the growth of gravity wave amplitude (Fritts et al., 2006). The positive temperature bias can be explained by a number of reasons. First, there might be deviations of the real atmospheric conditions for a given period from that modeled by the GCM. It is known that there were at least two major dust storm events during the considered time period (Smith, 2004): one at $L_s=225°$ and one at $L_s=260°$ that might be the cause for large temperature deviation shown in Fig. 7b. Second, the positive temperature bias may be caused by offsets in the TES retrievals. One cannot assign these offsets to uncertainties of the non-LTE model since those only affect the upper part of the retrieval domain. One should also rule out the retrieval algorithm issues since, as the self-consistency study shows (see Section 4), it can introduce only minor disturbances to the temperature profile. The offset may be caused by radiance calibration issues like the vertical field of view wing shape or by the spectra selection procedure. A radiance leak from below would be barely noticeable if the vertical radiance gradients are low. However, if an area with low temperatures and pressures is observed then the contributions of lower layers become important (Rezac, 2011). Positive bias in our TES retrievals can also be linked with the limb sequence selection criteria described in Section 3.2. Using a selecting procedure that discards the scans with low SNR may also filter out the low temperature cases that are characterized by low radiance values.

6. Conclusion

We have described a non-LTE model and algorithm that is applied to the temperature retrieval using the 15 μm limb geometry emissions measured by the TES instrument. We used integrated limb radiance in the 560–770 cm⁻¹ spectral range to increase the SNR and to extend the retrievals up to ~90 km altitude. We applied a forward fitting retrieval algorithm and showed that it provides a stable solution that does not depend on the initial guess profile. The combined uncertainty of the temperature retrieval due to noise and algorithm implementation is estimated to be 2 K at 60 km and below, 4 K at 70 km, 7 K at 80 km, 10 K at 85 km, and 20 K at 90 km altitude. Performing the retrievals from the integrated TES radiance produces temperature profiles similar to those measured by other instruments and predicted by models. Overall, ~1200 individual limb sequences have been selected, processed, and provided for download by the community. The temperature profiles retrieved from TES at 60 – 90 km altitude were compared to corresponding profiles from the Mars Climate Database. In general, good qualitative agreement between the two datasets was observed. A positive bias of TES retrieved temperatures with respect to MCD temperatures was found that varies from 6 K at 60 km to 11.5 K at 90 km. We explain this bias both by natural atmospheric

variability and by the filtering out of some low temperature profiles in our signal selection routine. The standard deviation of our retrieved temperature profiles compared to the MCD varies from ±20 K at 60 km to ±31 K at 90 km, which is explained by gravity wave growth with altitude as well as by larger retrieval uncertainties at higher altitudes. In summary, this study shows how to extend the limits of the already highly capable TES instrument, and validates the general concepts built in to Martian GCMs.

Acknowledgements

Appendix: Abbreviations used in text

ALI-ARMS: Accelerated Lambda Iterations for Atmospheric Radiation and Molecular Spectra

CRISTA: CRyogenic Infrared Spectrometers and Telescopes for the Atmosphere

GCM: General Circulation Model

HITRAN: HIgh-resolution TRANsmission molecular absorption database

LTE: Local Thermodynamic Equilibrium

MGS: Mars Global Surveyor

MY24: Martian Year 24, Mars Climate Database scenario characterized by low dust conditions

NER: Noise Equivalent Radiance

SABER: Sounding of the Atmosphere using Broadband Emission Radiometry

SNR: Signal to Noise Ratio

TES: Thermal Emission Spectrometer

TIMED: Thermosphere Ionosphere Mesosphere Energetics and Dynamics

VMR: Volume Mixing Ratio

References

Castle, K. J., K. M. Kleissas, J. M. Rhinehart, E. S. Hwang, and J. A. Dodd, Vibrational relaxation of $CO_2(v_2)$ by atomic oxygen, J. Geophys. Res., 111, A09303, doi:10.1029/2006JA011736, 2006.

Christensen, P. R., J. L. Bandfield, V. E. Hamilton, S. W. Ruff, H. H. Kieffer, T. N. Titus, M. C. Malin, R. V. Morris, M. D. Lane, R. L. Clark, B. M. Jakosky, M. T. Mellon, J. C. Pearl, B. J. Conrath, M. D. Smith, R. T. Clancy, R. O. Kuzmin, T. Roush, G. L. Mehall, N. Gorelick, K. Bender, K. Murray, S. Dason, E. Greene, S. Silverman, and M. Greenfield, Mars Global Surveyor Thermal Emission Spectrometer experiment: Investigation description and surface science results, J. Geophys. Res., 106(E10), 23,823–23,871, 2001.

Clancy, R.T., M.J. Wolff, P.R. Christensen. Mars aerosol studies with the MGS TES emission phase function observations: optical depths, particle sizes, and ice cloud types vs latitude and solar longitude. J. Geophys. Res., 108, doi:10.1029/2003JE002058.

Conrath, B. J., J. C. Pearl, M.D. Smith, W. C. Maguire, S. Dason, M. S. Kaelberer, and P. R. Christensen, Mars Global Surveyor Thermal Emission Spectrometer (TES) observations:

Atmospheric temperatures during aerobraking and science phasing, 2. Geophys. Res., 105, 9509–9520, 2000.

Feofilov, A.G., Kutepov, A.A., Pesnell, W.D., Goldberg, R.A., Marshall, B.T., Gordley, L.L., García-Comas, M., López-Puertas, M., Manuilova, R.O., Yankovsky, V.A., Petelina, S.V., and Russell III, J. M., Daytime SABER/TIMED observations of water vapor in the mesosphere: retrieval approach and first results, Atmos. Chem. Phys., 9, 8139–8158, 2009.

Forbes, J.M., Miyahara, S., Solar semidiurnal tide in the dusty Mars atmosphere. J. Atmos. Sci. 63(7), 1798–1817, 2006.

Forget, F., Hourdin, F., Fournier, R., Hourdin, C., Talagrand, O., Collins, M., Lewis, S.R., Read, P.L., Huot, J.-P., Improved general circulation models of the martian atmosphere from the surface to above 80 km. J. Geophys. Res. 104, 24,155–24,176, 1999.

Fritts, D. C., L. Wang, and R. H. Tolson, Mean and gravity wave structures and variability in the Mars upper atmosphere inferred from Mars Global Surveyor and Mars Odyssey aerobraking densities, J. Geophys. Res., 111(A12304), doi:10.1029/2006JA011897, 2006.

Gordley, L.L and J.M. Russell III, Rapid inversion of limb radiance using an emissivity growth approximation, Appl. Opt. 20, 807–813, 1981.

Grossmann, K. U., Offermann, D., Gusev, O., Oberheide, J., Riese, M., and Spang, R.: The CRISTA-2 mission, J. Geophys. Res., 107(D23), 8173–8185, doi:10.1029/2001JD000667, 2002.

Gusev O.A.: Non-LTE diagnostics of infrared observations of the planetary atmospheres. Ph.D. thesis, University of Munich, http://deposit.ddb.de/cgi-bin/dokserv?idn=968893651&dok_var=d1&dok_ext=pdf&filename=968893651.pdf, 2003.

Gusev, O., Kaufmann, M., Grossmann, K.U., Schmidlin, F.J., and Shepherd, M.G.: Atmospheric neutral temperature distribution at the mesopause/turbopause altitude, J. Atmos. Sol.-Terr. Phy., 68(15), 1,684–1,697, doi:10.1016/j.jastp.2005.12.010, 2006.

Gusev, O.A. and Kutepov, A.A.: Non-LTE gas in planetary atmospheres, in book: Stellar Atmosphere Modeling, I.Hubeny, D.Mihalas, and K.Werner, Eds., ASP Conference Series, 288, 318–330, 2003.

Hartogh, P., Medvedev, A.S., Jarchow, C., Middle atmospheric polar warmings on Mars: Simulations and study on the validation with submillimeter observations, Adv. Space Res. 55, 1103–1112, 2007.

Heavens, N. G., M.I. Richardson, W.G. Lawson, C. Lee, D.J. McCleese, D.M. Kass, A. Kleinböhl, J.T. Schofield, W.A. Abdou, J.H. Shirley, Convective instability in the martian middle atmosphere, Icarus, 208, 574–589, 2010.

Houghton, J.T., Taylor, F.W., and Rodgers, C.D, Remote soundings of atmospheres, Cambridge University Press, Cambridge, New York, Series title: Cambridge planetary science series, 343 pp, 1984, republished 2009.

Kaufmann, M., Gusev, O.A., Grossmann, K.U., Roble, R.G., Hagan, M.E., Hartsough, C., and Kutepov, A.A.: The vertical and horizontal distribution of CO_2 densities in the upper mesosphere and lower thermosphere as measured by CRISTA, J. Geophys. Res., D107, 8182, 10.1029/2001JD000704, 2002.

Kaufmann, M., Gusev, O.A., Grossmann, K.U., Martin-Torres, F.J., Marsh, D.R., and Kutepov, A.A.: Satellite observations of day- and nighttime ozone in the mesosphere and lower thermosphere, J. Geophys. Res., 108D, 10.1029/2002JD002800, 2003.

Khvorostovskaya, L. E., I.Yu. Potekhin, G.M. Shved, V.P. Ogibalov, and T.V. Uzyukova, Izvestiya Atmos. Ocean. Phys., 38, 613–624, 2002.

Kutepov, A.A., Gusev, O.A., and Ogibalov, V.P.: Solution of the non-LTE problem for molecular gas in planetary atmospheres: Superiority of accelerated lambda iteration, J. Quant. Spectrosc. Ra., 60, 199–220, 1998.

Kutepov, A.A., Feofilov, A.G., Marshall, B.T., Gordley, L.L., Pesnell, W.D., Goldberg, R.A., and Russell, J.M., III: SABER temperature observations in the summer polar mesosphere and lower thermosphere: importance of accounting for the CO_2 v_2-quanta V–V exchange, Geophys. Res. Lett., 33, L21809, doi:10.1029/2006GL026591, 2006.
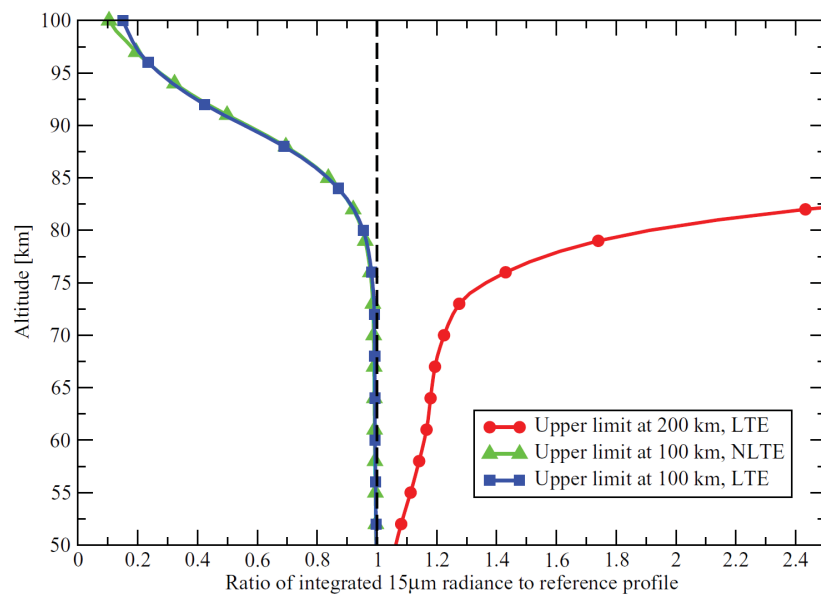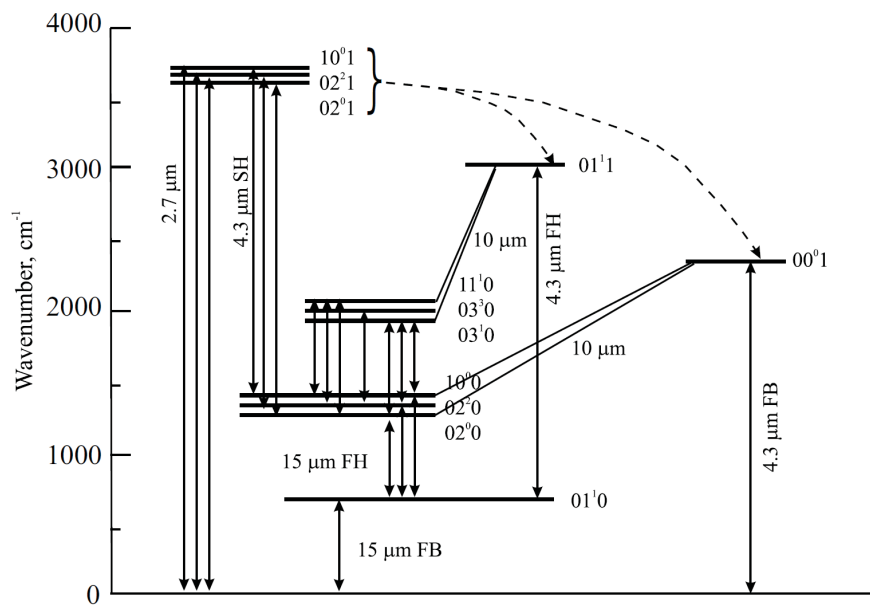
López-Puertas, M. and Taylor, F.W.: Non-LTE Radiative Transfer in the Atmosphere, World Scientific Publishing Co., River Edge, N.J., 504pp, 2001.
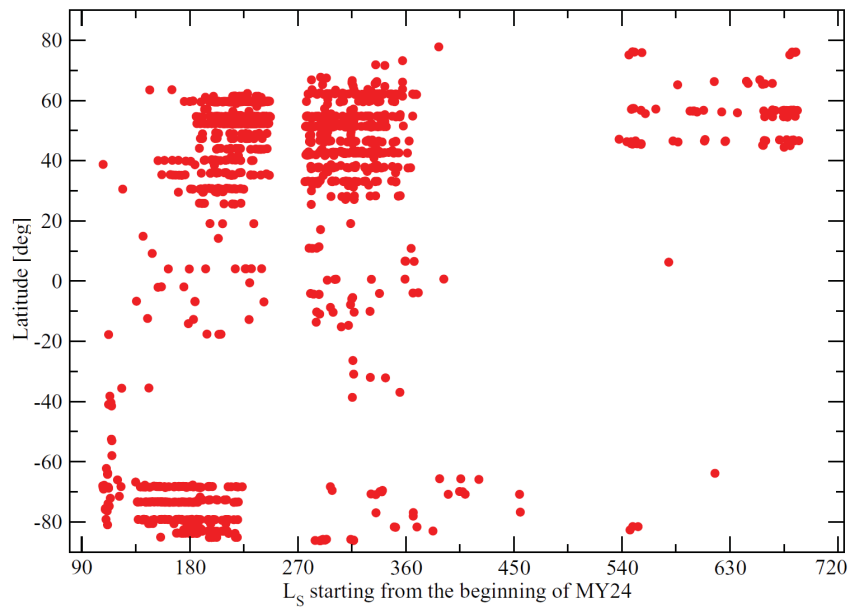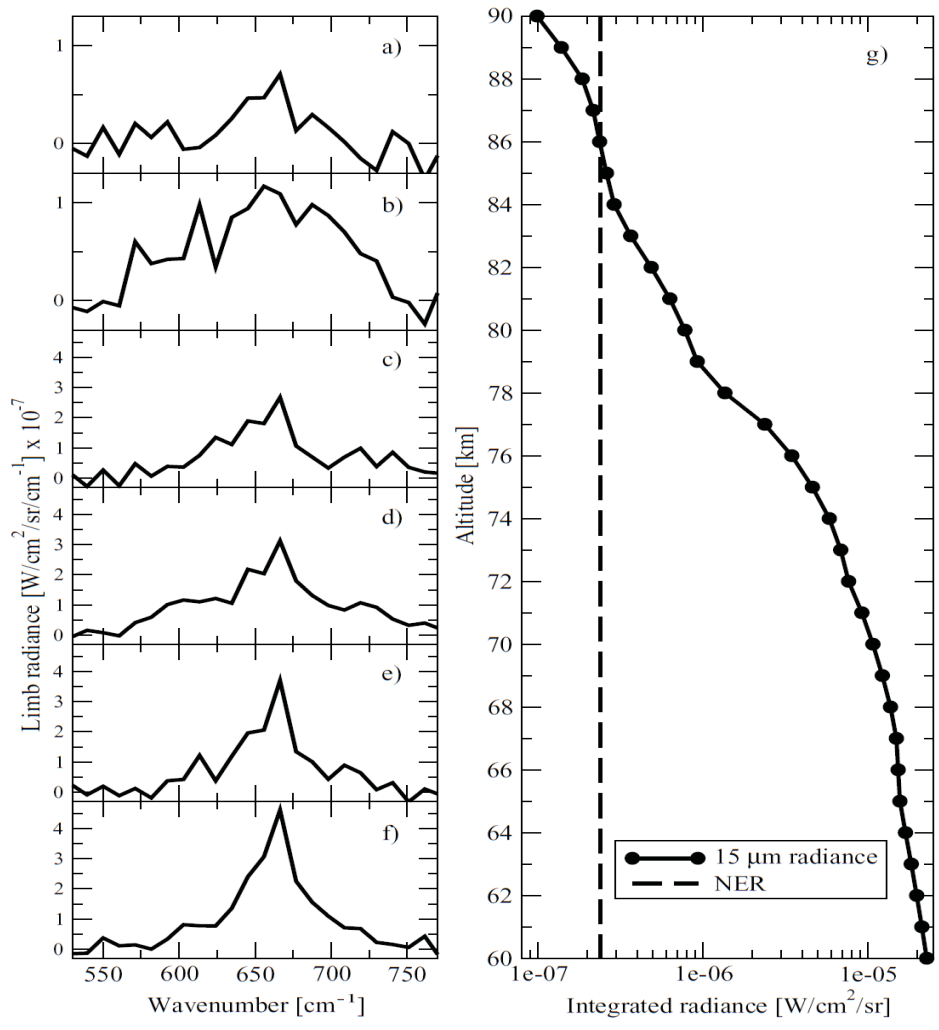
Offermann, D., Grossmann, K.U., Barthol, P., Knieling, P., Riese, M., and Trant R.: Cryogenic Infrared Spectrometers and Telescopes for the Atmosphere (CRISTA) experiment and middle atmosphere variability, J. Geophys. Res., 104, 16,311–16,325, 1999.
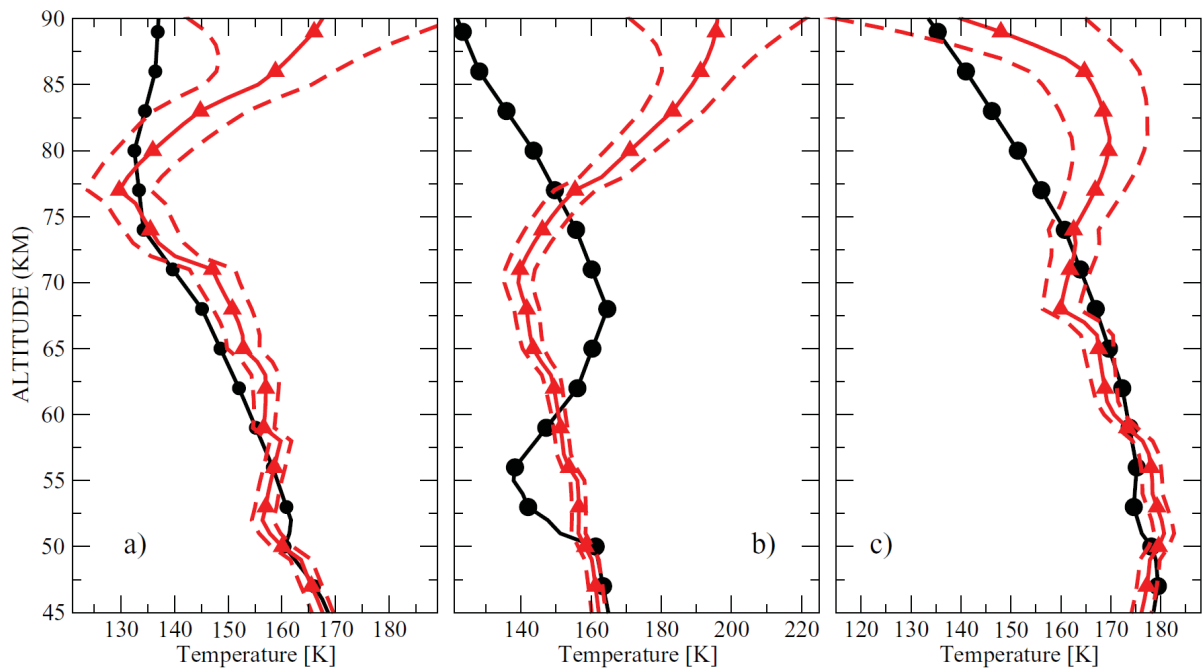
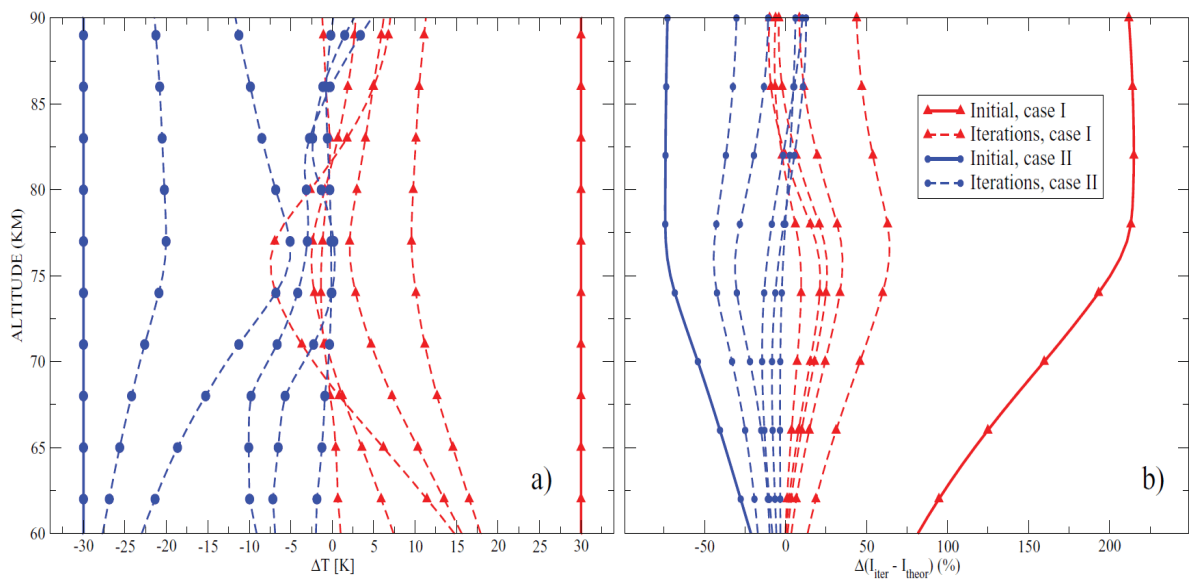Pearl, J. C., M. D. Smith, B. J. Conrath, J. L. Bandfield, and P. R. Christensen, Observations of water-ice clouds by the Mars Global Surveyor Thermal Emission Spectrometer experiment: The first martian year, J. Geophys. Res., 12,325-312,338, 2001.

Pollock, D. S., G.B.I.Scott and L.F. Phillips, Rate constant for quenching of CO_2(010) by atomic oxygen, Geophys. Res. Lett., 20, 727–729, 1993.

Ratkowski, A. J., et al., Lower-thermospheric infra-red emissions from minor species during high-latitude twilight–B. Analysis of 15 μm emission and comparison with non-LTE models, J. Atm. Terr. Phys., 56, 1899–1914, 1994.

Rezac, L., Simultaneous retrieval of T(p) and CO_2 volume mixing ratio from limb observations of infrared radiance under non-LTE conditions, Ph.D. thesis, Hampton University of Virginia, 163 pp, 2011.

Rothman, L.S., D. Jacquemart, A. Barbe, D.C. Benner, M. Birk, L.R. Brown, et al., The HITRAN 2004 molecular spectroscopic database. J. Quant. Spect. Rad. Transf., 96, 139-204, 2005.

Russell III, J. M., M.G. Mlynczak, L.L. Gordley, J. J. Tansock, and R. Esplin, Overview of the SABER experiment and preliminary calibration results, Proc. SPIE, Opt. Spectr. Tech. and Instrum. for Atm. and Space Res. III, 3756, 277–288, 1999.

Rybicki, G. B. and Hummer, D. G.: An accelerated lambda iteration method for multilevel radiative transfer. I - Non-overlapping lines with background continuum, Astron.Astrophys., 245, 171–181, 1991.

Sharma, R. D., and P. P. Wintersteiner, Role of carbon dioxide in cooling planetary thermospheres, Geophys. Res. Lett., 17, 2201–2204, 1990.

Smith, M. D., J. C. Pearl, B. J. Conrath, and P. R. Christensen, Thermal Emission Spectrometer results: Mars atmospheric thermal structure and aerosol distribution, J. Geophys. Res., 106, 23929-23945, 2001.

Smith, M. D., The annual cycle of water vapor on Mars as observed by the Thermal Emission Spectrometer, J. Geophys. Res., 197, 5115, doi:5110.1029/2001JE001522, 2002.

Smith, M. D., Interannual variability in TES atmospheric observations of Mars during 1999-2003, Icarus, 167, 148-165, 2004.

Wolff, M.J., and R.T. Clancy. Constraints on the size of Martian aerosols from Thermal Emission Spectrometer observations. J. Geophys. Res., 108, doi:10.1029/2003JE002057, 2003.

Wavenumber, cm^{-1}

4000

10^01
02^21
02^01

2.7 μm

4.3 μm SH

01^11

10 μm

4.3 μm FH

11^10
03^30
03^10

10^00
02^20
02^00

10 μm

00^01

4.3 μm FB

3000

2000

1000

15 μm FH

01^10

15 μm FB

0

Altitude [km]

100
95
90
85
80
75
70
65
60
55
50

Upper limit at 200 km, LTE
Upper limit at 100 km, NLTE
Upper limit at 100 km, LTE

0   0.2   0.4   0.6   0.8   1   1.2   1.4   1.6   1.8   2   2.2   2.4

Ratio of integrated 15μm radiance to reference profile

Limb radiance [W/cm^2/sr/cm^{-1}] x 10^{-7}

Wavenumber [cm^{-1}]

Altitude [km]

Integrated radiance [W/cm^2/sr]

- ● - 15 μm radiance
- - - - NER

Latitude [deg]
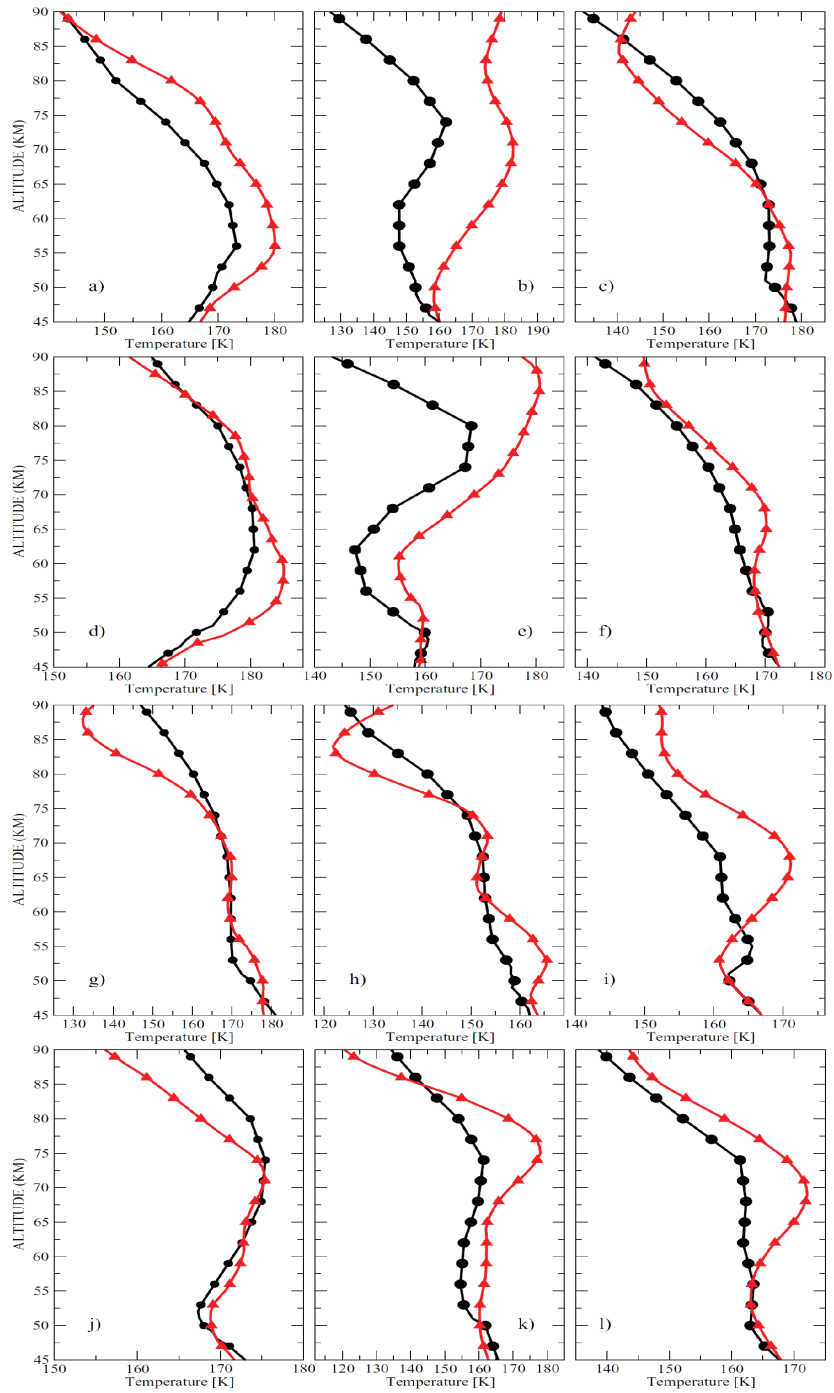
L_S starting from the beginning of MY24

Fig. 1. Scheme of vibrational level and major energy exchange processes for CO_2 and its isotopes. Solid lines: radiative transitions, dashed lines: V–V energy transfer from solar pumped levels. V–T processes are not shown. FB: fundamental band; FH: first hot band; SH: second hot band.

Fig. 2. Changes in the integrated 15 µm radiance using the $L_s = 180°$, lat = 0° Mars Climate Database atmospheric profile. Test runs were performed for LTE conditions in the atmosphere set up to 200 km (circles), non-LTE conditions in the atmosphere cut off at 100 km (triangles), and LTE conditions in the atmosphere cut off at 100 km (squares).

Fig. 5. Self-consistent retrievals of the temperature profile $T_{ref}(z)$ in the $60 - 90$ km altitude range: a) iterations starting with two different initial guess temperature profiles: $T(z) = T_{ref}(z) - 30$ K (case I) and $T(z) = T_{ref}(z) + 30$ K (case II); b) percent difference between the reference and calculated radiance profiles in the course of iterations for cases I and II.

Fig. 3. MGS TES spectra over 530–770 cm^{-1} at: a) 88.6 km; b) 82.6 km; c) 75.6 km; d) 71.4 km; e) 68.2 km; f) 60.8 km. Panel g) shows the 15 µm radiance integrated over the 560–772 cm^{-1} spectral range. Noise equivalent radiance (NER) was estimated from the points outside the integration interval: 508–560 cm^{-1} and 772–825 cm^{-1}.

Fig. 4. Seasonal and latitudinal coverage of the MGS TES limb sequences satisfying the selection criteria.

Fig. 6. Temperature retrieval examples: a) L_s=110°, lat = –62°; b) L_s=135°, lat = –6°; c) L_s=180°, lat = 59°. Curves with circles: initial temperature profile (MGS-TES below 50 km; MCD above 50 km). Curves with triangles: temperature retrievals performed in this work. Dashed lines: error bars for temperature retrievals.

Fig. 7. Zonally (±2.5°) and seasonally (±15°) averaged temperature retrievals from MGS-TES integrated 15 µm CO_2 radiances. Curves with circles: reference temperature profile (MGS-TES below 50 km; MCD above 50 km). Curves with triangles: temperature retrievals performed in this work: a) L_s=240°, lat = –73°; b) L_s=240°, lat = –7° (note the larger temperature difference perhaps due to a dust storm); c) L_s=240°, lat = 64°; d) L_s=270°, lat = –79°; e) L_s=270°, lat = 25°; f) L_s=270°, lat = 64°; g) L_s= 360°, lat = –68°; h) L_s=360°, lat = 20°; i) L_s=360°, lat = 69°; j) L_s=390°, lat = –88°; k) L_s=390°, lat = –24°; l) L_s=390°, lat = 64°.